IV Escola de Primavera de Transição e Turbulência
Universidade Federal do Rio Grande do Sul
Pontifícia Universidade Católica do Rio Grande do Sul
Porto Alegre, RS, 27 de setembro a 1° de outubro de 2004

The Turbulent Boundary Layer Subject to a Rough-to-Smooth Surface Change

Wagner M. Brasil
Mechanical Engineering Program (PEM/COPPE/UFRJ)
C.P. 68503, 21945-970, Rio de Janeiro, Brazil
e-mail wbrasil@mecanica.coppe.ufrj.br

Su Jian
Nuclear Engineering Program (PEN/COPPE/UFRJ)
C.P. 68509, 21945-970, Rio de Janeiro, Brazil

Atila P. Silva Freire
Mechanical Engineering Program (PEM/COPPE/UFRJ)
C.P. 68503, 21945-970, Rio de Janeiro, Brazil
e-mail atila@mecanica.coppe.ufrj.br

Abstract. *In this work, the statistical and the mean properties of a boundary layer subject to a rough-to-smooth step change in surface will be studied. The particular interesting property of this flow is the slow recovery in characteristics following the change in surface roughness. The result is the establishement of a flow where the rough-wall dominates the rate of diffusion of the disturbances for a considerable length, dictating conditions that are far from self-preserving. The hot-wire anemometry is our selected measuring technique. A hot-wire anemometer is a low cost equipment with a very high frequency response, relative small size, low noise levels, high accuracy and a continuous analogur signal. For this reason, it is the ideal instrument for measurements in low and moderate turbulence intensity flows.*

Keywords: *Statistical properties, turbulence, boundary layer, roughness, thermal-anemometry.*

1. Introduction

The purpose of this work is to investigate the mean and the statistical properties of a boundary layer subject to a rough-to-smooth step change in surface. The resulting flow is a particularly good test case for the study of non-equilibrium conditions. Indeed, in the early seventies, Antonia and Luxton (1971), Antonia and Luxton (1972) and Antonia et al. (1977) showed that for rough-to-smooth surface transitions the rate of diffusion of the disturbances is dominated by the rough-wall conditions for a considerable length. Thus, this slow recovery in flow properties following the change establish conditions that are not self-preserving.

An interesting question that soon comes to mind, then, concerns the behaviour of the error in origin. The error in origin is a well established concept since the sixties when it was solidly established by Perry and Joubert (1963), Perry et al.(1969) and Perry et al. (1987). In a classic paper, Perry and Joubert (1963) reviewed many rough-wall boundary layer investigations in order to correlate resistance to a characteristic length of the flow, the distance below the top of the roughness elements, also known as the error in origin, ε. The result was the development of a graphical method that has been used since then to determine the local boundary layer characteristics from each measured velocity distribution. The Perry and Joubert graphical method was further put to proof and improved on two following publications, Perry et al.(1969) and Perry et al. (1987). Some years later, Jackson (1981) provided a better physical interpretation to the displacement height showing that it could be regarded as the level at which the mean drag on the surface appears to act. Jackson also showed that the displacement height coincides with the displacement thickness for the shear stress.

Thus, the question we were referring to before is the following. In the non-equilibrium region following the surface change when we have already a smooth surface but the flow keeps part of the memory it had acquired over the rough surface, what is the behaviour of the error in origin? How does it recovers to its equilibrium value? Can a standard numerical computation of the flow based on a classical algebraic turbulence model capture this behaviour?

All this questions are of great relevance in view of the extensive use of the law of the wall and, consequently, of the error in origin, for the evaluation of the skin-friction coefficient. In fact, Avelino and Silva Freire (2002) and Loureiro and Silva Freire (2004) have shown that much remains to be understood about the error in origin for turbulent flows over rough surfaces.

While many works turned their attention on investigations to the mean properties of the flow, others have studied the statistical properties (Ligrani and Moffat (1985), Perry et al. (1987), Bandyopadhyay (1987), Krogstad and Antonia (1994)). Here we we also investigate some of the statistical properties of a boundary layer subject to a rough-to-smooth step change in surface. It is a fact that the recent development of computational fluid dynamics has placed a strong emphasis on the accurate measurement of mean velocity components and of Reynolds stresses. However, the fundamental statistical approach to turbulence analysis still plays a central role in the understanding of complex flows.

The chief measuring technique to be employed here will be the hot-wire anemometry. A hot-wire anemometer is a low cost equipment with a very high frequency response, relative small size, low noise levels, high accuracy and a continuous analogur signal. For this reason, there is no surprise such equipments are judged ideal for measurements in low and moderate turbulence intensity flows.

2. The error in origin

For flows over surfaces, where the roughness elements have a height much superior to the viscous region length scale, ν/u_τ, the viscous sublayer is completely destroyed by the protuberances at the wall. Under this condition, the fully turbulent region has to suffer some adjustments so as to yield a good description of the velocity and the temperature fields. Some authors, Perry and Joubert (1963), Perry et al.(1969) and Perry et al. (1987), have shown that a universal expression can be written for the wall region provided the origin for measuring the velocity profile is set at some distance below the crest of the roughness elements. This displacement in origin is referred to in literature as the error in origin, ε.

Thus, for any kind of rough surface, it is possible to write

$$\frac{u}{u_\tau} = \frac{1}{\varkappa} \ln\left[\frac{(z_T + \varepsilon)u_\tau}{\nu}\right] + A - \frac{\Delta u}{u_\tau}, \tag{1}$$

where,

$$\frac{\Delta u}{u_\tau} = \frac{1}{\varkappa} \ln\left[\frac{\varepsilon u_\tau}{\nu}\right] + C_i, \tag{2}$$

$\varkappa = 0.4$, $A = 5.0$, and $C_i, i = K, D$; is a parameter characteristic of the roughness.

Equations 1 and 2, although of a universal character, have the inconvenience of needing two unknown parameters for their definition, the skin–friction velocity, u_τ, and the error in origin, ε. A chief concern of many works on the subject is, hence, to characterize these two parameters.

For an experimentalist, however, these equations are very useful for they provide a graphical method for the determination of the skin-friction coefficient.

3. The one-dimensional spectrum

The three-dimensional energy spectrum is one of the key concepts in turbulence theory (Tennekes and Lumley (1972)). However, in the laboratory, researchers find it much more convenient to measure the longitudinal spectrum. This, of course, sets the problem of relating the measured one-dimensional spectrum to the theoretical three-dimensional spectrum.

If a one dimensional flow has its movement captured by a hot-wire anemometer, then the velocity fluctuations may be decomposed into their harmonic components in respect to the angular frequency, ω. Then, by analyzing and averaging the signal, the resulting frequency spectrum, $E_{11}(\omega)$ must have the property

$$\left\langle {u_1'}^2 \right\rangle = \int_0^\infty E_{11}(\omega) d\omega. \tag{3}$$

To relate the frequency and wavenumber spectra, the common practice is to use the 'frozen convection' hypothesis of Taylor that considers the changes in u_1 with time at a fixed point to be due to the passage of a frozen pattern of turbulent motion.

This is equivalent to state

$$u(x,t) = u(x - \overline{u_1}t, 0), \tag{4}$$

or else,

$$\frac{\partial}{\partial t} = -\overline{u_1}\frac{\partial}{\partial x_1}. \tag{5}$$

The Taylor hypothesis is still open to scrutiny even today, but it is at least a very good approximation and hence will be used extensively here.

Defining

$$E_{11}(k_1) = \overline{u_1}E_{11}(\omega), \quad k_1 = \omega/\overline{u_1}. \tag{6}$$

Then, it follows that

$$\int_0^\infty E_{11}(\omega)d\omega = \int_0^\infty \frac{E_{11}(k_1)d\omega}{\overline{u_1}} = \int_0^\infty E_{11}(k_1)dk_1 = \left\langle {u_1'}^2 \right\rangle. \tag{7}$$

An extension of the above equation to three dimensions is trivial, it suffices to integrate out the dependence of $E_{11}(k_1)$ on k_2 and k_3 to obtain

$$E(k) = \frac{k^3 d[k^{-1}dE_{11}(k)/dk]}{dk}. \tag{8}$$

4. Time domain analysis

The output signal of a hot-wire anemometer is random by its very nature (Bruun (1995)). Therefore, a statistical description of its contents is in order. Next we will very briefly remind the reader some of the basic concepts in random data analysis and introduce the paper notation.

The autocorrelation function for the flow velocity is denoted by R_u, the autocorrelation coefficient function by ρ_u and the auto-spectral density function by S_u.

Consider a time-history velocity record, u. It can be split into a mean, $\overline{u}$ and a fluctuating component, u',through

$$u(t) = \overline{u} + u' \tag{9}$$

where the mean value is the average of all values, defined by

$$\overline{u} = lim_{T\to\infty}\frac{1}{T}\int_0^T u(t)\,dt. \tag{10}$$

In a digital data analysis, the continuous signal is replaced by a digital sample record. Taking T as the total sample time and N the corresponding number of samples, the sampling rate is given by $S_R = N/T = N\,F$.

Thus, the mean value of a finite sample record, $u(j)$, j = 1,2,..., N can be given by

$$\overline{u} = \frac{1}{N}\sum_{j=1}^{N} u(n). \tag{11}$$

The autocorrelation function shown the dependence of the data at one time in relation to the values at another time. An estimate of the autocorrelation function with a time delay $\tau = r/F$ can be written as

$$R_u(r/F) = \frac{1}{N-r}\sum_{j=1}^{N-r}\left[u(j)-\bar{u}\right]\left[u(j+r)-\bar{u}\right], \quad r = 0,1,2,\cdots,m. \tag{12}$$

where r is the lag number and m is the maximum lag number.

The autocorrelation coefficient function is defined by

$$\rho_u(r/F) = \frac{R_u(r/F)}{R_u(0)}. \tag{13}$$

The autospectral density function is defined in terms of a Fourier transform of the previously calculated correlation function

$$S_u(f) = \int_{-\infty}^{\infty} R_u(\tau) e^{-i2\pi f\tau}\, d\tau. \tag{14}$$

The autospectral density function can also be evaluated from a finite Fourier transform of the data record. Define

$$S_x(f,T,k) = \frac{1}{T} u_k^*(f,T) u_k(f,T), \tag{15}$$

where

$$u_k(f,T) = \int_0^T u_k(t) e^{-i2\pi ft}\, dt. \tag{16}$$

Quantity $u_k(f,T)$ represents a finite Fourier transform of $u_k(t)$ and * denotes the complex conjugate. Then, $S_u(f)$ can be defined by

$$S_u(f) = \lim_{T\to\infty} E\left[S_x(f,T,k)\right], \tag{17}$$

where $E\left[S_x(f,T,k)\right]$ is the expected value by taking the ensemble average.

Here the autospectrum was estimated by computing an ensemble of estimates from different subrecords. This procedure drastically reduces the autospectrum random error.

The corresponding integral time-scale for the autocorrelation function is given by

$$Ti_u = \int_0^{\infty} \rho_u(\tau) d\tau. \tag{18}$$

The integral times scales give a measure of the time separation in which the two fluctuating parameters $u'(t)$ and $u'(t+\tau)$ are correlated with themselves. So that two signals can be considered statistically uncorrelated we must have a time interval between samples of the order of $\tau = 2Ti$.

The second order moments, also called the variance, is given by

$$\sigma_u^2 = \overline{u'\ u'} = \frac{1}{Nn_u - 1}\left\{\sum_{j=1}^{Nn_u} \left[u(j)\right]^2 - Nn_u\ \bar{u}^2\right\} \tag{19}$$

The turbulent intensity is given by

$$Tu = \frac{\sqrt{\overline{u'\ u'}}}{\bar{u}}, \tag{20}$$

The third and forth order moments, also known as the skewneess and the kurtosis, or flatness factor, are given by

$$\sigma_u^2 = \overline{u'\ u'} = \frac{1}{Nn_u - 1}\left\{\sum_{j=1}^{Nn_u} \left[u(j)\right]^2 - Nn_u\ \bar{u}^2\right] \tag{21}$$

and

$$\sigma_u^4 = \frac{1}{Nn_u}\left\{\sum_{j=1}^{Nn_u}[u(j)]^4 - 4\bar{u}\sum_{j=1}^{Nn_u}[u(j)]^3 + 6\bar{u}^2\sum_{j=1}^{Nn_u}[u(j)]^2 - 3\ Nn_u\ \bar{u}^4\right\} \tag{22}$$

The uncertainties (P=99) associated with the measured statistical quantities are given by

$$\bar{u}(\theta) = \bar{u} \pm \frac{2,57}{\sqrt{Nn_u}}\bar{u}\ Tu \tag{23}$$

$$\overline{u'(\theta)\ u'(\theta)} = \overline{u'\ u'} \pm 2,57\frac{\overline{u'\ u'}}{\sqrt{Nn_u}}. \tag{24}$$

$$\overline{u'(\theta)\ u'(\theta)\ u'(\theta)} = \overline{u'\ u'\ u'} \pm 2,57\left(\overline{u'\ u'}\right)^{3/2}\sqrt{\frac{6}{Nn_u}}. \tag{25}$$

$$\overline{u'(\theta)\ u'(\theta)\ u'(\theta)\ u'(\theta)} = \overline{u'\ u'\ u'\ u'} \pm 2,57\left(\overline{u'\ u'}\right)^2\sqrt{\frac{96}{Nn_u}}. \tag{26}$$

5. Small scales

Although the large eddies contribute to most of the transport of momentum and scalars, we know viscous dissipation of turbulence to be determined by the smallest of the eddies.

In this section, we will show how the smallest length scales in a turbulent flow can be found (Tennekes and Lumley (1972)).

Consider that small-scale motions have small time scales, which are statistically independent of the large scales. This argument leads to the conclusion that the rate of energy suply should equal the rate of dissipation. This is the basis of Kolmogorov's universal equilibrium theory. This theory suggests that the microscales of length, time and velocity are given by

$$\eta = \left(\frac{\nu^3}{\varepsilon}\right)^{1/4}, \qquad \varphi = \left(\frac{\nu}{\varepsilon}\right)^{1/2}, e \qquad \upsilon = (\nu\varepsilon)^{1/4}. \tag{27}$$

The autocorrelation coefficient defines a further important microscale, Λ_u, which is defined by the curvature of ρ_u at the origin:

$$\left.\frac{d^2\rho_u(\zeta)}{d\zeta^2}\right|_{\zeta=0} = -\frac{2}{\Lambda_u^2} \tag{28}$$

The length scale Λ_u is called the Taylor time microscale; it is directly associated with the dissipation rate in a turbulent flow.

Expanding $\rho_u(\zeta)$ in a Taylor series around the origin, we can write for small values of ζ,

$$\rho_u(\zeta) \cong 1 - \frac{\zeta^2}{\Lambda_u^2}. \tag{29}$$

To correlate the Taylor time microscale with the longitudinal spectrum, we make

$$\overline{\left(\frac{du'}{dt}\right)^2} = 2\frac{\overline{u'u'}}{\Lambda_u^2}. \tag{30}$$

Then, applying Taylor hypothesis to the above equation,

$$\overline{\left(\frac{du'}{dx}\right)^2} = \frac{2}{\bar{u}^2}\frac{\overline{u'u'}}{\Lambda_u^2}. \tag{31}$$

The Taylor length microscale, χ_u, is given by

$$\overline{\left(\frac{du'}{dx}\right)^2} = \frac{\overline{u'u'}}{\chi_u^2}, \tag{32}$$

and the following relation holds

$$\chi_u = \frac{\bar{u}}{\sqrt{2}}\Lambda_u \tag{33}$$

Finally, considering the turbulence isotropic, the dissipation rate, ϵ, can be evaluated from

$$\epsilon = 15\nu\frac{\overline{u'\ u'}}{\chi_u^2}. \tag{34}$$

6. Data reduction

As mentioned in the introduction, the present study resorted to the hot-wire anemometry to measure the properties of the turbulent flow. To accounted for any temperature variation, a temperature-compensated Dantec probe, model 55P76, was used. This probe consists of two sensor elements: a hot-wire and a resistance-wire, usually called cold-wire, situaded 2 mm below and 5 mm downstream of the former. Both sensors are Pt-plated tungsten wires, 5 μm in diameter, overall length of 3mm and sensitive wire length of 1,25 mm. They are copper and gold plated at the ends to approximately 30 μm. They were connected respectively to a constant temperature bridge, Dantec 55M10 and to a constant current brigde, Dantec 56C20.

Reference measurements for velocity were obtained from a Pitot tube connected to an inclined manometer; temperature reference data was obtained from previously calibrated microthermocouples.

The temperature dependence of the thermal anemometer signal was accounted for by the linear correction method, where the heat transfer from the probe is assumed to be proportional to a product of the temperature difference $T_w - T_a$ and a function of the velocity, where T_w is the temperature of the heated wire and T_a is the ambient temperature. The output voltage, E, of a constant temperature hot-wire anemometer can hence be represented by:

$$E^2 = f(U)(T_w - T_a). \tag{35}$$

Temperature measurements with resistance wires require both low drift, low noise constant current anemometers and high quality amplifiers. If the resistance wire is heated by a current $I = 0.15mA$, then the "hot" resistance R_w will only deviate from R_a by $(R_w - R_a)/R_a \simeq 0.0004$, and the corresponding temperature difference $(T_w - T_a)$ will be less than 0.1 ^oC.

Thus, a common practice is to consider $R_w = R_a$, with

$$R_a = R_0\,[1 + \alpha_0(T_a - T_o)]. \tag{36}$$

For practical applications, it is recommended that a temperature calibration of the resistance-wire is used to determine the calibration constants in the relationship

$$R_a = A + B\,T_a. \tag{37}$$

To establish the velocity and temperature sensitivity of the hot-wire probe operating at a fixed hot resistance, R_w, the anemometer output voltage, E_w, was red as a function of the velocity, U, and the fluid temperature, T_a. This type of calibration is often carried out by performing a velocity calibration at a number of different fluid temperatures.

The functional form of the calibration data was then written as

$$E = F(U, T_a - T_w)_{T_w = const}. \tag{38}$$

Equation 38 is a very good approximation to the velocity calibration data, obtained at a constant value of T_a, provided the calibration constants are determined by a least-squares curve fit. This procedure has been applied by other authors to their velocity calibration data using the wire voltage relationship

$$\frac{E_w^2}{R_w\,(R_w - R_a)} = A + BU^n. \tag{39}$$

This curve-fitting procedure gave the most accurate results. When a constant value of $n(= 0.45)$ was selected, A and B also became constants, and the increase in the uncertainty is insignificant for most hot-wire anemometry aplications.

The sampling rate was 2500 Hz, and the total measuring time for each point, 53 seconds.

7. Experimental facilities

The low-velocity, stratified-flow, wind tunnel used in this work was described in detail in Cataldi et al.(2001, 2002) and in Loureiro et al. (2001). The tunnel main objective is to simulate stratified atmospheric boundary layers. Some improvements have been recently made in the tunnel to achieve a better representation of atmospheric flows and similarity conditions. The test section has now an overall length of 10 m, with a cross section area of 0.67 m x 0.67 m. The position of the roof is ajustable so as to produce different pressure gradients. The potencial velocity of the wind tunnel varies from zero to 3,5 m/s, and the free stream has a turbulence intensity of about 2%.

The stratification section, consisting of 10 eletrical resistances, is capable of heating the flow differentially up to 100 ^oC; each of the resistances can be controlled individually. Following the heating section, the floor temperature can also be raised by 100 ^oC over a 6m long surface, by a series of resistances with a controlled variation of 5^oC. The total heating capacity of each panel is about 7 kW/m^2.

The flow was subjected to a step change in roughness (from rough-to-smooth) after travelling the first six meters over a rough wall. The rough surface consisted of roughness elements constructed from equally spaced transversal rectangular slats. The dimensions of the roughness elements were K (= 4.7625 mm), where denotes the height, S (= 15.875 mm) the length, W (= 15.875 mm) the gap, and λ (= 31.75 mm) the pitch. In constructing the surface, extreme care was taken to keep the first roughness element always depressed below the smooth surface, its crest kept aligned with the smooth glass wall surface.

The glass surface was always kept at 25 $^oC \pm 0.5$ ^oC. The next 6 meters, fitted with the rough surfaces, had their temperature raised to 75 $\pm$ 3 ^oC. In fact, the variation in surface temperature for most of the plates was very small, within $\pm$ 1 ^oC. However, the plates were manufactured in such a way that, at the junction (over a length of 10 cm), conjugated effects resulted in a small decrease in temperature (– 3 ^oC). The wall temperature was controlled by 15 thermocouples, set at five stream-wise stations at three span-wise positions.

8. Results

To determine the velocity error in origin, ε, the method of Perry and Joubert (1963) was used. Thus, velocity profiles were plotted in semi-log graphs in dimensional coordinates. Next, the normal distance from the top of the roughness elements was incremented by 0.1 mm and a straight line fit was applied to the resulting points. The best fit was chosen by searching for the maximum coefficient of determination, R-squared. Others statistical parameters were also observed, the residual sum of squares and the residual mean square. Normally, a coefficient of determination superior to 0.99 was obtained.

The determination of ε is illustrated in Figure 1.

Having found ε, we can then use the gradient of the log-law to determine u_τ. Another method to obtain u_τ is the momentum integral equation. This latter method, however, is very sensitive to any three-dimensionality of the flow and the determination of the derivatives of the various mean flow parameters is a highly inaccurate process.

To recover to the classical undisturbed values, the error in origin is observed to relax over 50 cm, the equivalent to about five boundary layer thicknesses. This value is quite different from the data reported in Antonia and Luxton (1972) where more than 16 boundary layer thicknesses were necessary for the flow to return to a self-preserving state. Thus the behaviour of the error in origin seems to be somehow detached from the behaviour of the Reynolds stresses that are much slower in responding changes in wall conditions.

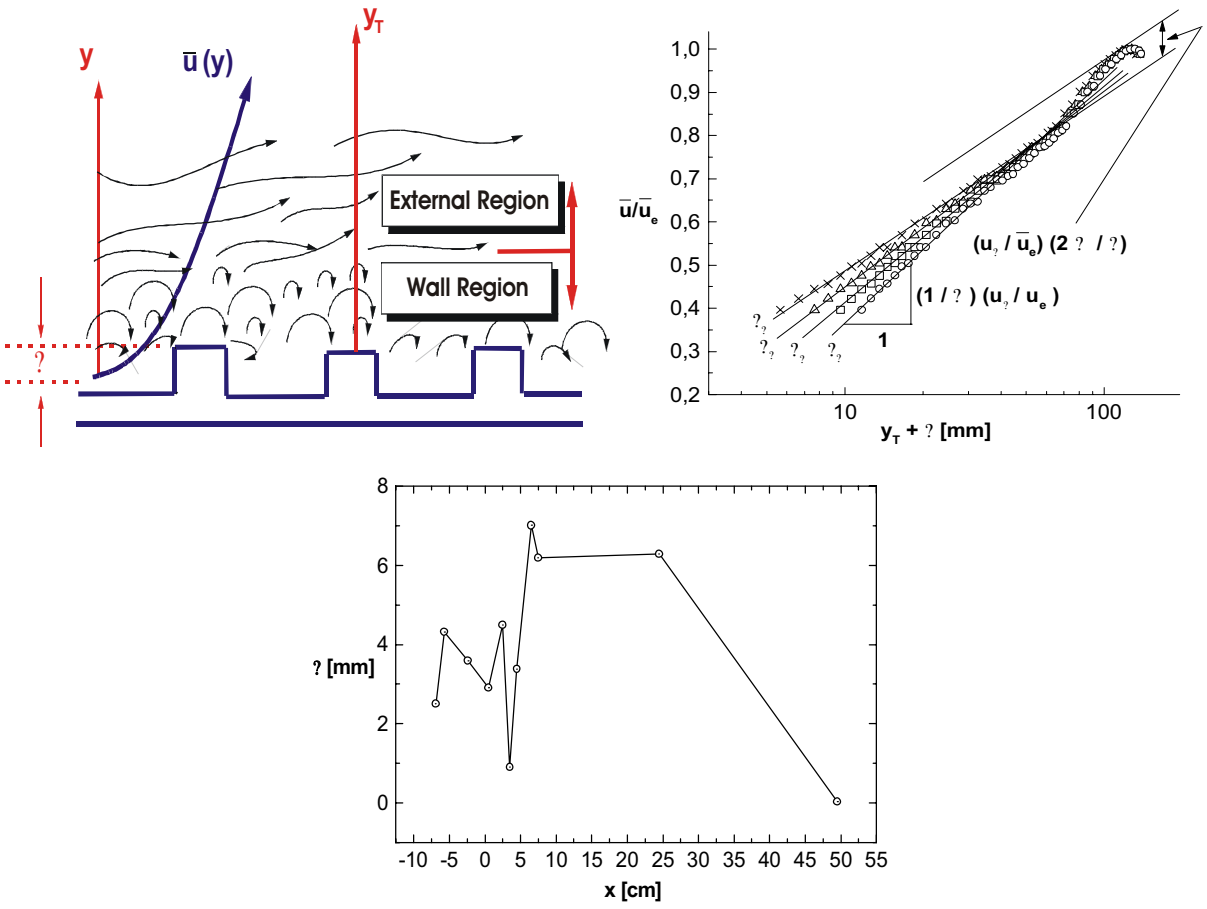

Figure 1: The determination of ε.

The next figures illustrate the changes in the statistical properties of a fluid passing over a sudden rough-to-smooth change in surface condition.

The autocorrelation function, Figure 2, shows that for measurements taken with a time shift over 0.2 seconds the data were uncorrelated. This number is quite different from our smooth plate results where 0.05 seconds were necessary for data to be uncorrelated.

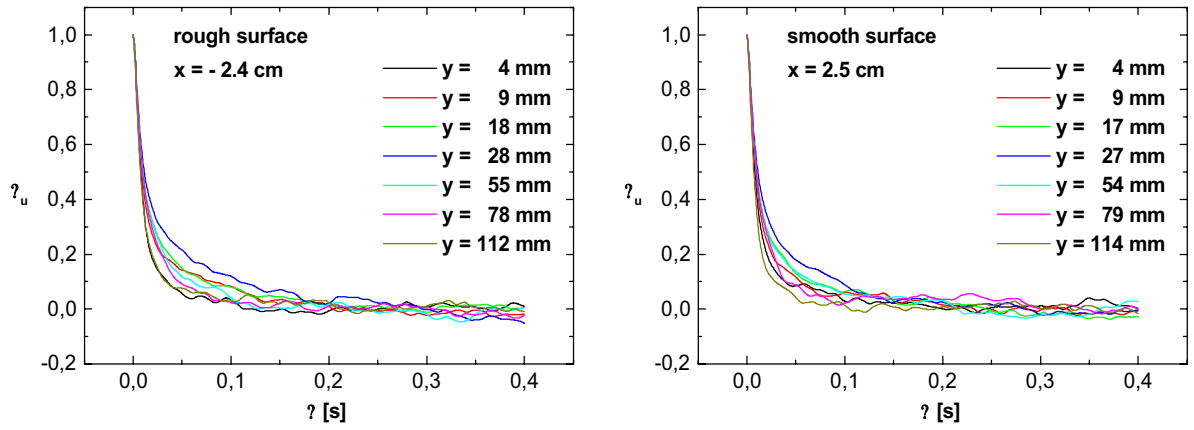

Figure 2: Autocorrelation function.

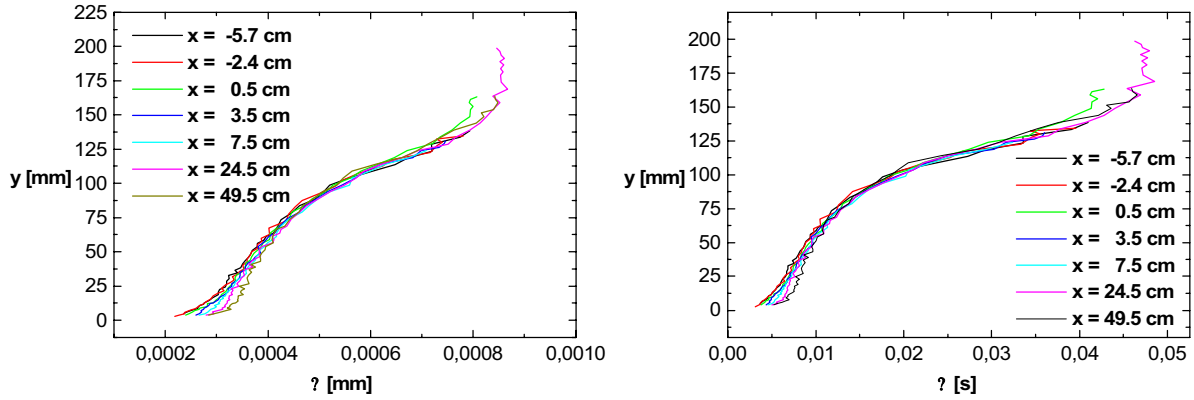

Figure 3: The Kolmogorov time and length scales. Curves were drawn for the following stations: x= -6,2, 0.5, 2.5, 5.5, 9.5 and 24.5 cm. The reference x=0 is the point of surface change.

The Kolmogorov scales, Figures 3 and 4, were shown to be virtually independent of the flow transition regime. Thus, they do not present any significant longitudinal variation. This same trend is followed by the scales of Taylor, Fig. 5, and by the turbulent energy dissipation, 6.

The major changes in flow conditions are illustrated by the higher-moments and the energy spectra, Figures 7, 8 and 9. These graphs clearly show the roughness effects on the inner layer properties of the boundary layer.

The second-order moments are particularly affected by the upstream wall condition. For the whole x-wise distance, where the profiles were measured, a non-equilibrium condition was observed. The high turbulence levels originated at the rough wall showed a reasonably slow decay rate (Figure 7).

The third-order moments are negative in most of the outer region, and positive in the near-wall region. Also, because they are much the same for flows over smooth or rough walls, they tend to colapse onto a single line.

The same trend is observed for the forth-order moments; they are independent of the wall condition. Much as observed by Bandyopadhyay and Watson (1988), the peak occurs for y/δ of the order of 1.2, contrary to the data of other authors that show that for high Reynolds number the peak is achieved at 0.8. Thus we have found a peak at a position that has been determined by the upstream surface condition.

The spectra show clearly an inverse-power-law region where the Kolomogorov scaling can be identified. The -5/3 power law region could be well discriminated, showing the inertial subrange.

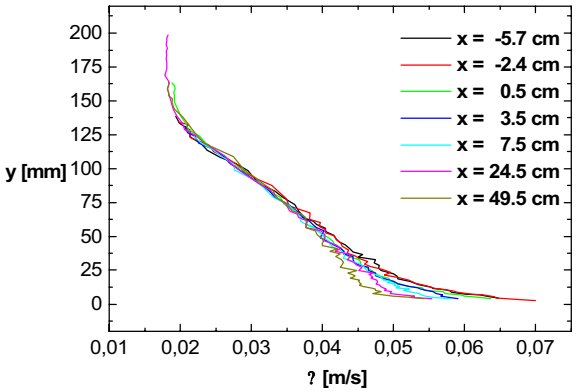

Figure 4: The Kolmogorov velocity scale. Curves were drawn for the following stations: x= -6,2, 0.5, 2.5, 5.5, 9.5 and 24.5 cm. The reference x=0 is the point of surface change.

After an integration over the various u_1-spectra regions, the u_1-broadband turbulence intensity distribution in the turbulent wall region can be written as

$$\frac{\overline{u_1^2}}{u_\tau^2} = B_1 - A_1 \ln \frac{y}{\delta} - C(yu_\tau/\nu)^{-1/2} \tag{40}$$

where C is a universal constant and B_1 is a large-scale characteristic constant.

The above equation is now under a further scrutiny from the authors so that the behaviour of B_1, A_1 and C can be investigated.

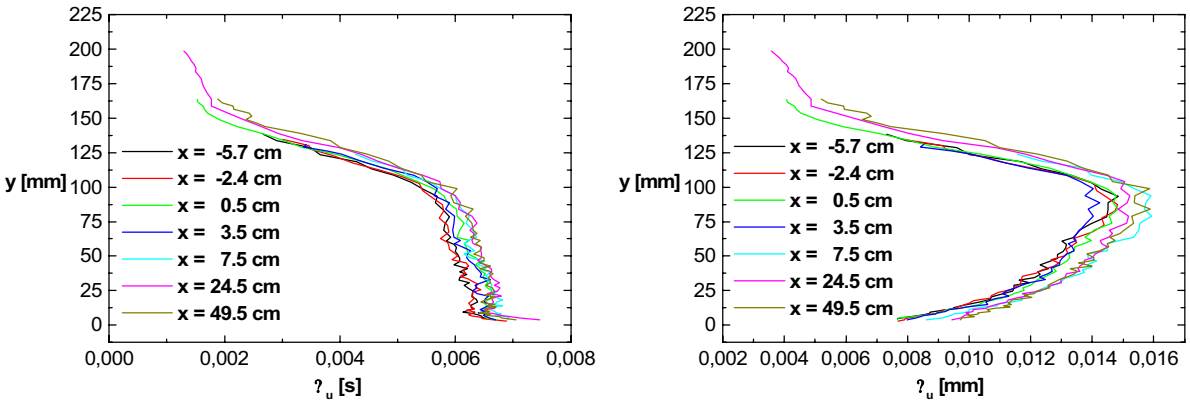

Figure 5: The Taylor time and length scales. Curves were drawn for the following stations: x= -6,2, 0.5, 2.5, 5.5, 9.5 and 24.5 cm. The reference x=0 is the point of surface change.

9. Final Remarks

The data presented in this paper have shown that soon after a change in surface properties, from rough to smooth, some of the statistical characteristics of the flow go through a slow recovery process. That is due to the fact that the rough-wall flow dominates the rate of diffusion of the disturbances for a considerable length, dictating conditions that are not self-preserving. The second-order moments are an example of this occurence.

On the other hand, the fact that the spectra suffers very little, or even none, influence of the roughness length scale is significant to illustrate that simple turbulence models will not be able to correctly simulate all the flow characteristics. In other words, we have shown that to try to characterize a flow over a rough surface by just modelling the effects that the protuberances have on the mean velocity or temperature profiles is simply not enough, more sophisticated models are needed.

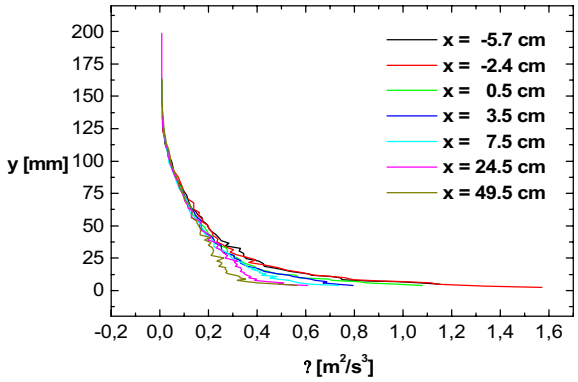

Figure 6: The turbulent energy dissipation. Curves were drawn for the following stations: x= -6,2, 0.5, 2.5, 5.5, 9.5 and 24.5 cm. The reference x=0 is the point of surface change.

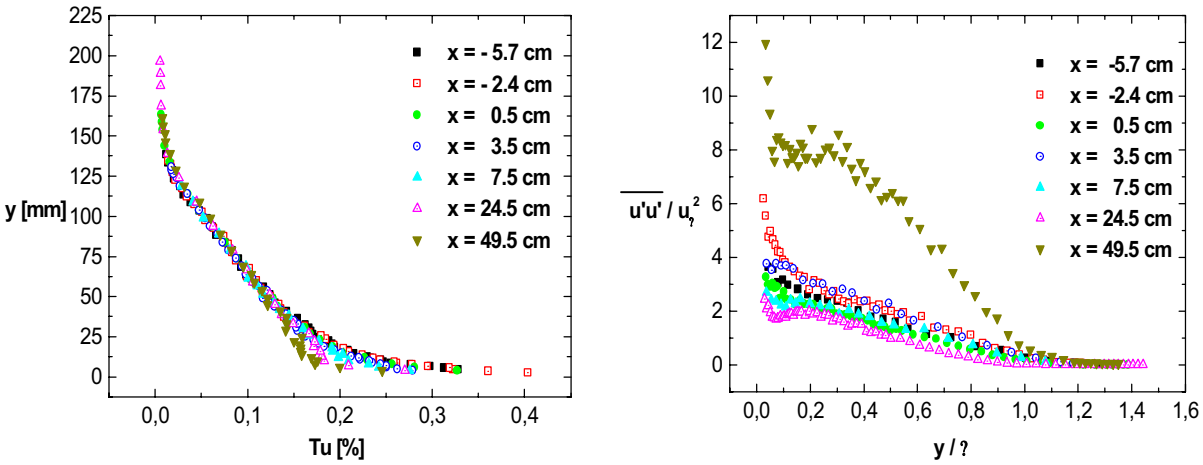

Figure 7: Turbulent intensity and longitudinal second-order moments.

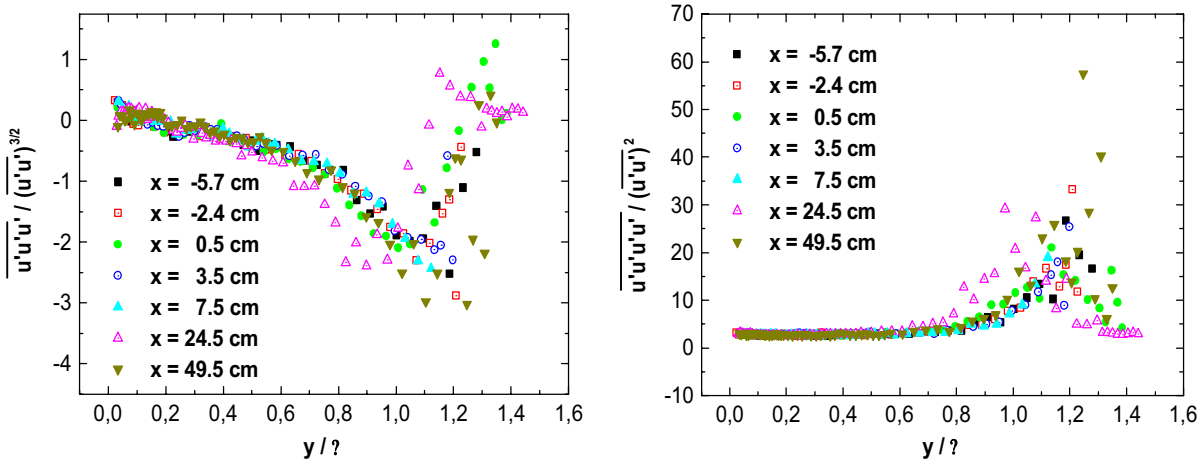

Figure 8: Longitudinal third- and forth-order moments.

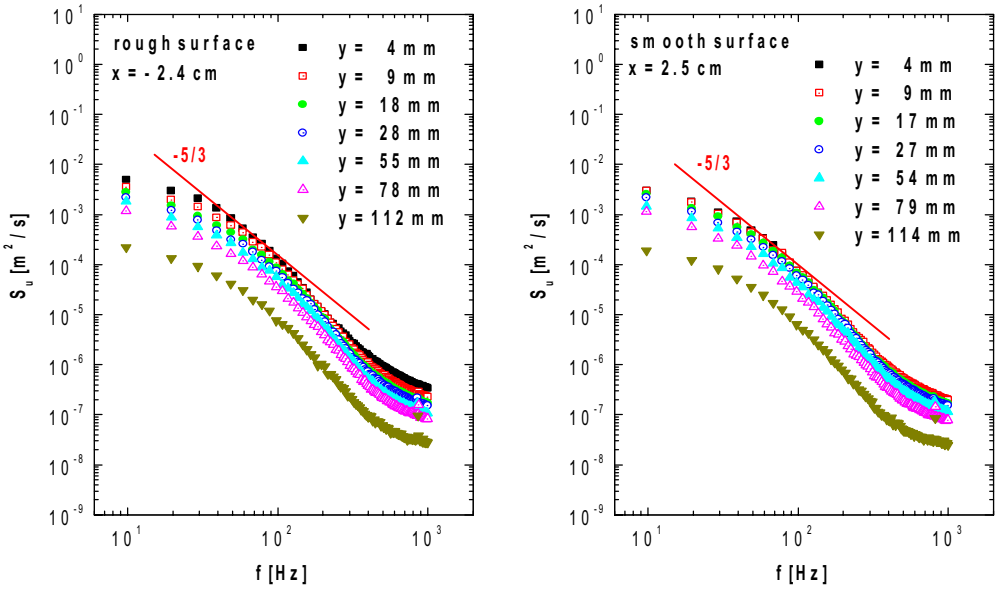

Figure 9: Energy spectra. Figures refer to the two following stations: x= -6.2 and 24.5 cm (left to right). Curves were drawn from top to bottom for the following heights: 4, 9, 18, 27, 54, 79, 111 cm.

Acknowledgements. APSF is grateful to the Brazilian National Research Council (CNPq) for the award of a research fellowship (Grant No 304919/2003-9). The work was financially supported by CNPq through Grant No 472215/2003-5 and by FAPERJ through Grants E-26/171.198/2003 and E-26/152.368/2002. SJ is also grateful to the CNPq and to Faperj for the award of research grants.

10. References

Avelino, M. R. and Silva Freire, A. P., 2002, On the displacement in origin for turbulent boundary layers subjected to sudden changes in wall temperature and roughness, Int. J. Heat and Mass Transfer, 45, 3145-3153.

Antonia, R.A. and Luxton, R.E., 1971, The response of a turbulent boundary layer to a step change in surface roughness. Part 1. Smooth to Rough, J. Fluid Mechanics, 48, 721–761.

Antonia, R.A. and Luxton, R.E., 1972,The Response of a Turbulent Boundary Layer to a Step Change in Surface Roughness Part 2. Rough to Smooth, J. Fluid Mechanics, 53, 737–757.

Antonia, R.A., Danh, W.H. and Prabhu, A., 1977, Response of a Turbulent Boundary Layer to a Step Change in Surface Heat Flux, J. Fluid Mechanics, 80, 153-177.

Bandyopadhyay, P.R., 1987, Rough Wall Turbulent Boundary Layers in the Transition Regime, J. Fluid Mechanics, 180, 231-266.

Bandyopadhyay, P.R. and Watson, R. D., 1988, Structure of rough-wall turbulent boundary layers, Phys. Fluids, 31, 1877-1883.

Bruun, H. H., 1995, Hot-wire Anemometry - Principles and Signal Analysis, Oxford University Press.

Cataldi, M., Loureiro, J. B. R., Pimentel, L. C. G. e Silva Freire, A. P., 2001, Design features and flow measurements in a thermally stratified wind tunnel", XVI Congresso Brasileiro de Engenharia Mecânica (COBEM), Uberlândia.

Cataldi, M., Loureiro, J. B. R., Pimentel, L. C. G. e Silva Freire, A. P., 2002, A comparison between wind tunnel simulation and field measurements of the atmospheric boundary layer", Anais do IX Congresso Brasileiro de Engenharia e Ciências Térmicas (ENCIT), Caxambu.

Krogstad, P.-A. and Antonia, R. A., 1994, Structure of turbulent boundary layers on smooth and rough walls, J. Fluid Mechanics, 277, 1-21.

Loureiro, J. B. R. e Silva Freire, A. P., 2004, 'Periodically Heated Turbulent Flow over a Rough Surface: Characteristics of the Error in Origin.", Encontro Nacional de Ciências Térmicas (ENCIT), Rio de Janeiro, Dezembro.

Perry, A.E. and Joubert, P. N., 1963, 'Rough-Wall boundary layers in adverse pressure gradients', *J. Fluid Mechanics* **17**, 193-211.

Perry, A.E., Schofield, W. H. and Joubert, P. N., 1969, 'Rough wall turbulent boundary layers', *J. Fluid Mechanics* **37**, 383-413.

Perry, A.E., Lim, K.L. and Henbest, S.M., 1987, An Experimental Study of the Turbulence Structure in Smooth- and Rough-Wall Boundary Layers, J. Fluid Mechanics, 177, 437–466.

Tennekes, H. And Lumley, J. L., 1972, A first course in turbulence, MIT Press.

P.M. Ligrani and R.J. Moffat, 1985, Thermal Boundary Layers on a Rough Surface Downstream of Steps in Wall Temperature, Boundary Layer Meteorology, 31, 127-147.